Anal. Chem. **2003,** *75,* 6202−6208

A Split-Field Drift Tube for Separation and Efficient Fragmentation of Biomolecular Ions

Stephen J. Valentine,[†] Stormy L. Koeniger,[‡] and David E. Clemmer*[,‡]

Beyond Genomics, 40 Bear Hill Road, Waltham, Massachusetts 02451, and Department of Chemistry, Indiana University, Bloomington, Indiana 47405

A new ion mobility instrument that incorporates a low-field region for ion separation and a high-field region for collisional activation is described. In this approach, mixtures of ions are separated based on differences in their mobilities in a ∼20-cm-long low-field (∼5 V cm^{-1}) region of a drift tube. As the ions approach the drift tube exit, they are exposed to a large focusing potential drop; at high fields, ions are efficiently collisionally activated and dissociate as they exit the drift tube. We have demonstrated this approach by examining the fragmentation pattern for electrosprayed bradykinin ions. These studies show that the activation process is highly tunable; it is possible to modulate the field such that precursor ion mass spectra as well as several high-field collision-induced fragmentation patterns can be obtained. The approach also appears to be a simple means of activating protein ions, as demonstrated by examining electrosprayed myoglobin ions.

Mass spectral fragmentation patterns obtained upon activating precursor ions provide a great deal of information about covalent structure, and these data have emerged as a key to determining the sequences of many types of biomolecules.[1−16] For this reason, the ability to predict and manipulate the accessibility of different pathways is of great interest and a number of promising methods of activation are emerging.[11,12,17−27] One simple approach that leads to substantial differences in fragmentation pathways is to vary the collision energy that is used for ion activation. For example, at low collision energies, peptide ions undergo cleavage of the peptide backbone—producing primarily b- and y-type fragment ions;[1,8,11,28,29] at high-collision energies (e.g., collisions with target gases or surfaces), fragmentation patterns become more complex as pathways for an array of fragment ions (a-, d-, and w-types as well as internal fragments) become accessible.[9,10,29,30] In this paper, we describe a simple ion activation method that can be carried out inside a drift tube. The approach energizes protein and peptide ions to a greater extent with less signal loss than that observed for low-energy collision-induced dissociation (CID) fragments produced immediately after the drift tube in an orifice skimmer cone region.[31,32] This high-field, CID method is tunable, yielding unique and highly reproducible fragmentation data sets for protein and peptide ion charge states. The ability to modulate fragmentation patterns at the exit of a drift tube presents opportunities for obtaining structural and sequence information in a very high-

* To whom correspondence should be addressed. E-mail: clemmer@indiana.edu.

† Beyond Genomics.

‡ Indiana University.

(1) Biemann, K. *Methods Enzymol.* **1990**, *193*, 351.
(2) Yost, R. A.; Boyd, R. K. *Methods Enzymol.* **1990**, *193*, 154.
(3) Gross, M. L. *Methods Enzymol.* **1990**, *193*, 131.
(4) Tober, K. B. *Mass Spectrom. Rev.* **1989**, *8*, 445.
(5) Biemann, K. *Biomed. Environ. Mass Spectrom.* **1988**, *16*, 99.
(6) Hunt, D. F.; Henderson, R. A.; Shabanowitz, J.; Sakaguchi, K.; Michel, H.; Sevilir, N.; Cox, A. L.; Appella, E.; Engelhard, V. H. *Science* **1992**, *255*, 1261.
(7) Hunt, D. F.; Michel, H.; Dickinson, T. A.; Shabanowitz, J.; Cox, A. L.; Sakaguchi, K.; Appella, E.; Grey, H. M.; Sette, A. *Science* **1992**, *256*, 1817.
(8) Ballard, K. D.; Gaskell, S. J. *Int. J. Mass Spectrom. Ion Processes* **1991**, *111*, 173.
(9) Johnson, R. S.; Martin, S. A.; Biemann, K.; Stults, J. T.; Watson, J. T. *Anal. Chem.* **1987**, *59*, 2621.
(10) Johnson, R. S.; Martin, S. A.; Biemann, K. *Int. J. Mass Spectrom. Ion Processes* **1988**, *86*, 137.
(11) McCormack, A. L.; Somogyi, Á.; Dongré, A. R.; Wysocki, V. H. *Anal. Chem.* **1993**, *65*, 2859.
(12) Jones, J. L.; Dongré, A. R.; Somogyi, Á.; Wysocki, V. H. *J. Am. Chem. Soc.* **1994**, *116*, 8368.
(13) Mortz, E.; O'Connor, P. B.; Roepstorff, P.; Kelleher, N. L.; Wood, T. D.; McLafferty, F. W.; Mann, M. *Proc. Natl. Acad. Sci. U.S.A.* **1996**, *93*, 8264.
(14) Cargile, B. J.; McLuckey, S. A.; Stephenson, J. L., Jr. *Anal. Chem.* **2001**, *73*, 1277.
(15) Speir, J. P.; Senko, M. W.; Little, D. P.; Loo, J. A.; McLafferty, F. W. *J. Mass Spectrom.* **1995**, *30*, 39.
(16) Little, D. P.; Speir, J. P.; Senko, M. W.; O'Connor, P. B.; McLafferty, F. W. *Anal. Chem.* **1994**, *66*, 2809.
(17) Chorush, R. A.; Little, D. P.; Beu, S. C.; Wood, T. D.; McLafferty, F. W. *Anal. Chem.* **1995**, *67*, 1042.
(18) Cooks, R. G.; Ast, T.; Mabud, MD. A. *Int. J. Mass Spectrom. Ion Processes* **1990**, *103*, 1.
(19) Mabud, MD. A.; Dekrey, M. J.; Cooks, R. G. *Int. J. Mass Spectrom. Ion Processes* **1985**, *67*, 285.
(20) Senko, M. W.; Beu, S. C.; McLafferty, F. W. *Anal. Chem.* **1994**, *66*, 415.
(21) Hunt, D. F.; Yates, J. F., III; Shabanovitz, J.; Winston, S.; Hauer, C. R. *Proc. Natl. Acad. Sci. U.S.A.* **1986**, *83*, 6233.
(22) Biemann, K.; Scoble, H. A. *Science* **1987**, *237*, 992.
(23) Schnier, P. D.; Price, W. D.; Jockusch, R. A.; Williams, E. R. *J. Am. Chem. Soc.* **1996**, *118*, 7178.
(24) Ge, Y.; Horn, D. M.; McLaffertyk, F. W. *Int. J. Mass Spectrom.* **2001**, *210*, 203.
(25) Little, D. P.; Speir, J. P.; Senko, M. W.; O'Connor, P. B.; McLafferty, F. W. *Anal. Chem.* **1994**, *66*, 2809.
(26) Price, W. D.; Schnier, P. D.; Williams, E. R. *Anal. Chem.* **1996**, *68*, 859.
(27) Freitas, M. A.; Hendrickson, C. L.; Marshall, A. G. *J. Am. Chem. Soc.* **1996**, *118*, 7390.
(28) Alexander, A. J.; Thibault, P.; Boyd, R. K. *Rapid Commun. Mass Spectrom.* **1989**, *3*, 30.
(29) Medzihradszky, K. F.; Maltby, D. A.; Qiu, Y.; Yu, Z.; Hall, S. C.; Chen, Y. Burlingame, A. L. *Int. J. Mass Spectrom. Ion Processes* **1997**, *160*, 357.
(30) Dongré, A. R.; Jones, J. L.; Somogyi, Á.; Wysocki, V. H. *J. Am. Chem. Soc.* **1996**, *118*, 8365.
(31) Lee, Y. J.; Hoaglund-Hyzer, C. S.; Taraszka, J. A.; Zientara, G. A.; Counterman, A. E.; Clemmer, D. E. *Anal. Chem.* **2001**, *73*, 3549−3555.

10.1021/ac030111r CCC: $25.00
Published on Web 10/10/2003

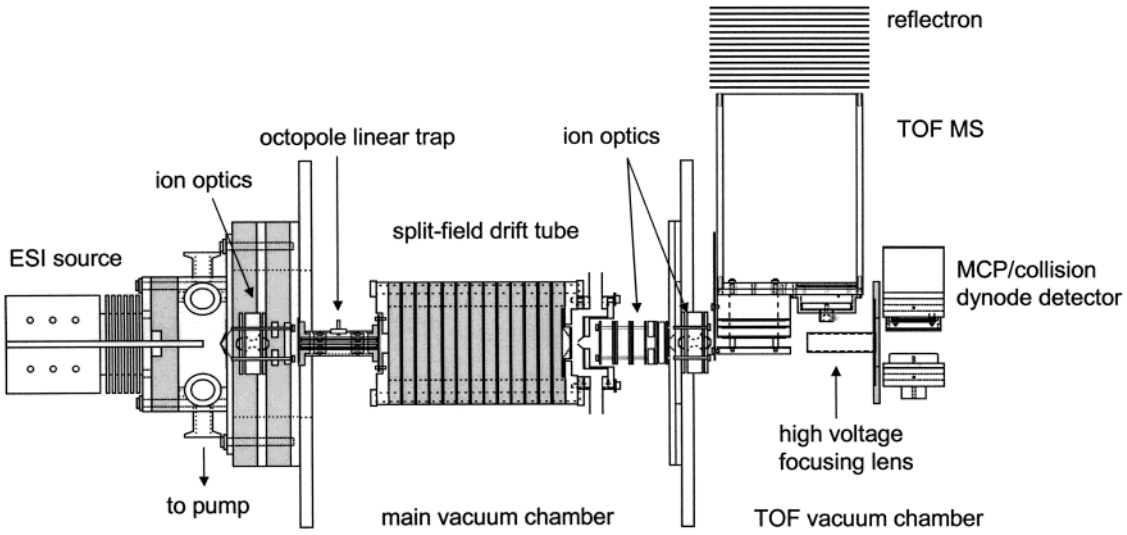

Figure 1. Schematic diagram of the split-field drift tube instrument.

throughput fashion. Here we illustrate this approach for the first time for a system of electrosprayed ions of the peptide bradykinin and a distribution of myoglobin charge states.

EXPERIMENTAL SECTION

General Overview. Detailed reviews of ion mobility techniques can be found elsewhere.[33−37] Figure 1 shows a schematic diagram of a new ion mobility/time-of-flight instrument that has been constructed in our laboratory. The instrument is similar to designs that we have described previously;[38,39] however, the chamber and pumping system are substantially smaller than in previous instruments. There are four main components: (1) an electrospray ionization (ESI)[40] source; (2) an octopole trap for accumulating the continuous ion beam; (3) a drift tube, in this case a design that incorporates a split low-/high-field design, which is discussed in more detail below; and (4) a time-of-flight mass spectrometer for ion detection. Briefly, experiments are conducted as follows. Ions formed by ESI are extracted into a high-vacuum region and focused into a linear octopole trap. The ion trap is cylindrically symmetric and comprises eight stainless steel rods that are enclosed in a stainless steel case and two end caps. The rf potentials applied to the rods combined with dc potentials at the end caps allow ions from the continuous source to be accumulated (for ∼6 ms in this study) into a packet and then injected into the drift tube. The drift tube is 21.90 cm long and is operated with a buffer gas pressure of 1.7 Torr. As discussed in more detail below, ions drift across most of the drift tube under the influence of a weak field (∼5 V·cm^{-1}) where they separate based on differences in their low-field mobilities through the buffer gas. The separated ions then enter a short region of the drift tube that can be operated at low or high field. When the exit region is operated at low fields, precursor ions are focused out of the drift tube. At high fields, the precursors undergo energizing collisions and may dissociate prior to being focused through the drift tube exit orifice. Upon exiting the drift tube, fragment ions (and remaining precursor ions) are focused into a time-of flight mass spectrometer and detected. As described previously, flight times in the mass spectrometer are much shorter than drift times, allowing mobilities and m/z information to be recorded in a nested fashion. We commonly refer to this as a nested drift(flight) time measurement—denoted as $t_D(t_F)$.[38]

Ion Formation. Bradykinin (98% purity, from Sigma) and myoglobin (equine, 90% purity from Sigma) were obtained and used without further purification. Positively charged (protonated) ions were produced by electrospraying solutions containing 2.4 $\times 10^{-4}$ M peptide or 2.9 $\times 10^{-6}$ M protein in 49:49:2 (% volume) water/acetonitrile/acetic acid. The solution flow rate was 1.3 μL·min^{-1}.

Split Low-/High-Field Injected-Ion Drift Tube Design. In the instrumental design (Figure 1), the drift tube is composed of concentric stainless steel rings that are isolated by Delrin spacers. The rings and spacers are stacked together, sealed with O-rings, and held into place by 16 nylon threaded rods that run along the outside of the rings. When compressed, the ring and spacer assembly creates a 21.90-cm-long chamber to which gas can be added. The diagram also shows the position of the ocotopole ion trap (which is mounted to the front lens plate of the drift tube) and a differentially pumped orifice skimmer region (at the back of the drift tube) that is similar in design to one described in detail previously. In all of the studies shown here, the orifice skimmer cone region is operated such that fragmentation in this region is

(32) Direct comparisons of the high-field ion fragmentation method with the orifice skimmer cone CID method have been carried out for several peptide ions (bradykinin, angiotensin I, angiotensin II, methionine enkephalin, substance P) as well as those produced from tryptic digestion of cytochrome *c*. Ion intensities in fragment spectra are more than 1 order of magnitude higher when recorded using the high-field fragmentation method. We also note that fragmentation efficiency in the high-field method appears to be greater for most ions.

(33) St. Louis, R. H.; Hill, H. H. *Crit. Rev. Anal. Chem.* **1990**, *21*, 321.
(34) Wyttenbach, T.; Bushnell, J. E.; Bowers, M. T. *J. Am. Chem. Soc.* **1998**, *120*, 5098.
(35) Clemmer, D. E.; Jarrold, M. F. *J. Mass Spectrom.* **1997**, *32*, 577.
(36) Hoaglund Hyzer, C. S.; Counterman, A. E.; Clemmer, D. E. *Chem. Rev.* **1999**, *99*, 3037.
(37) Jarrold, M. F. *Annu. Rev. Phys. Chem.* **2000**, *51*, 179.
(38) Hoaglund, C. S.; Valentine, S. J.; Sporleder, C. R.; Reilly, J. P.; Clemmer, D. E. *Anal. Chem.* **1998**, *70*, 2236−2242.
(39) Hoaglund-Hyzer, C. S.; Clemmer, D. E. *Anal. Chem.* **2001**, *73*, 177−184.
(40) Fenn, J. B.; Mann, M.; Meng, C. K.; Wong, S. F.; Whitehouse, C. M. *Science* **1989**, *246*, 64.

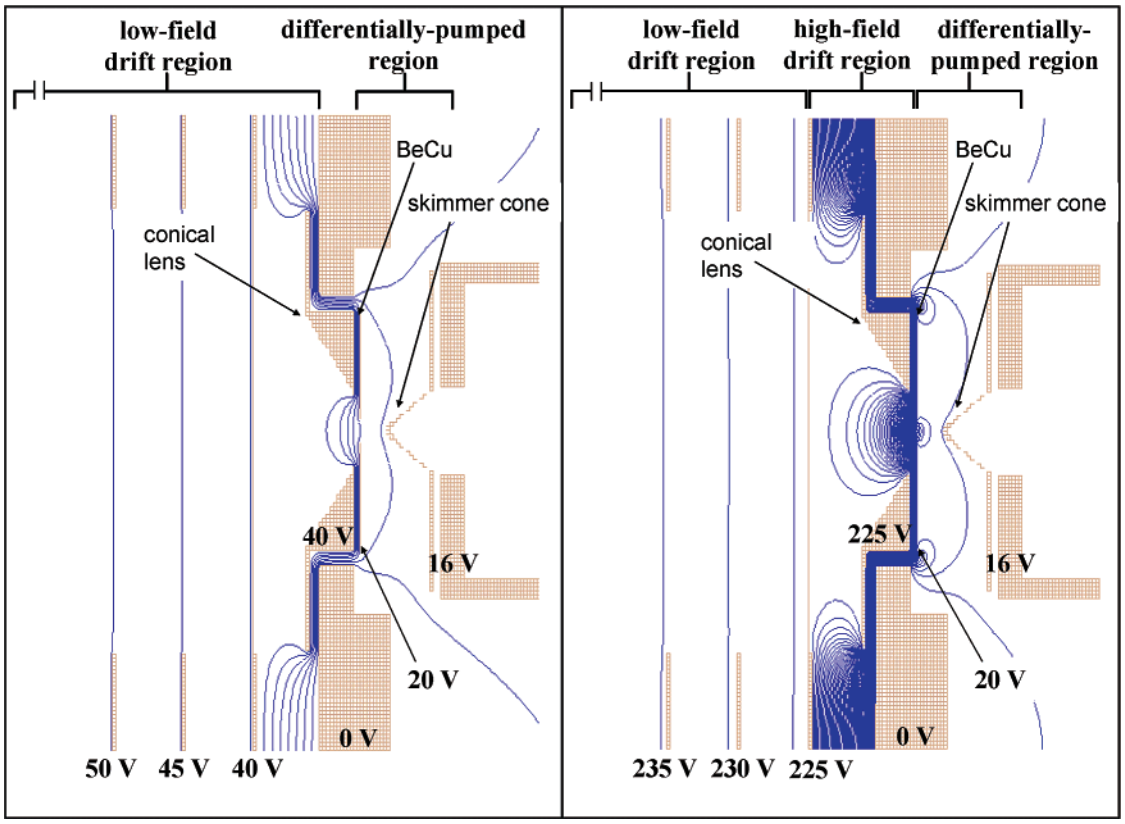

Figure 2. Cross section of the drift tube exit region with equipotential lines created from SIMION 7.0 (see ref 41). On the left and right are the equipotential lines for parent and fragment ion spectra (see text), respectively. The potential lines represent ~5 V. Low- and high-field regions are delineated as well as lens potentials.

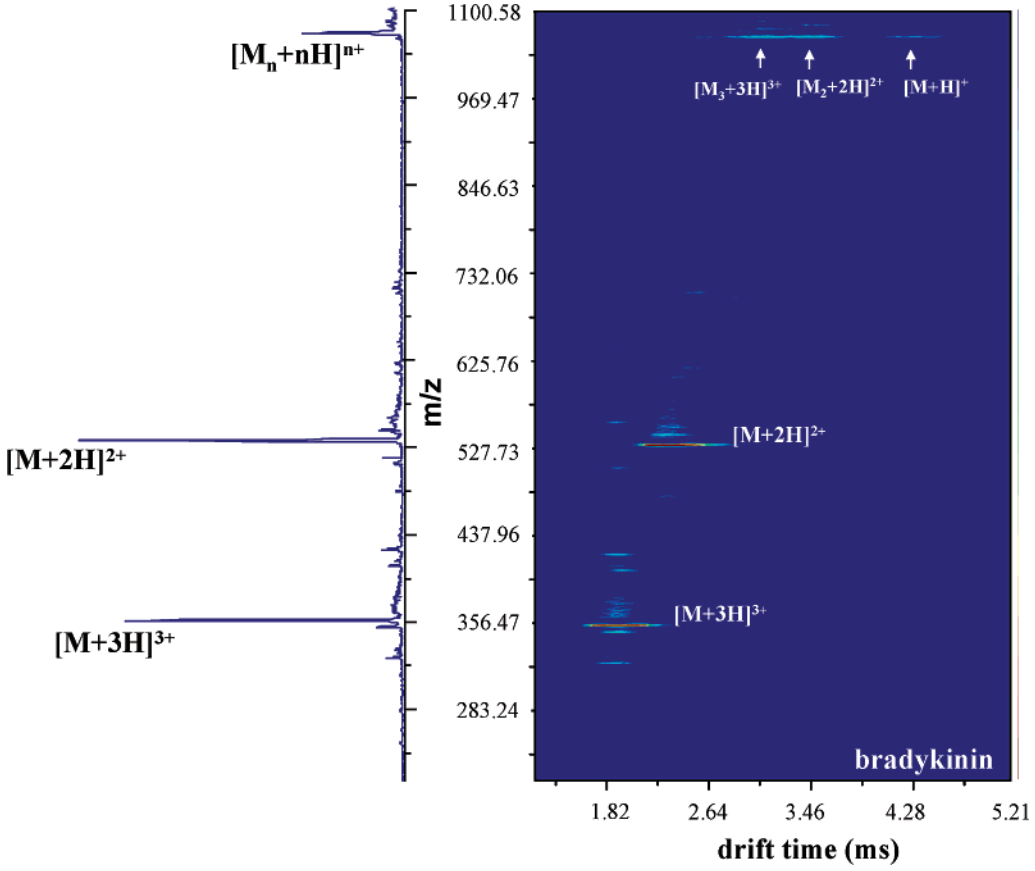

Figure 3. Contour plot of a nested drift(flight), parent ion data set for electrosprayed bradykinin ions. Monomer ion charge states as well as multimer ions are labeled. On the left is the mass spectrum obtained by summing all drift time bins at given *m*/*z* values.

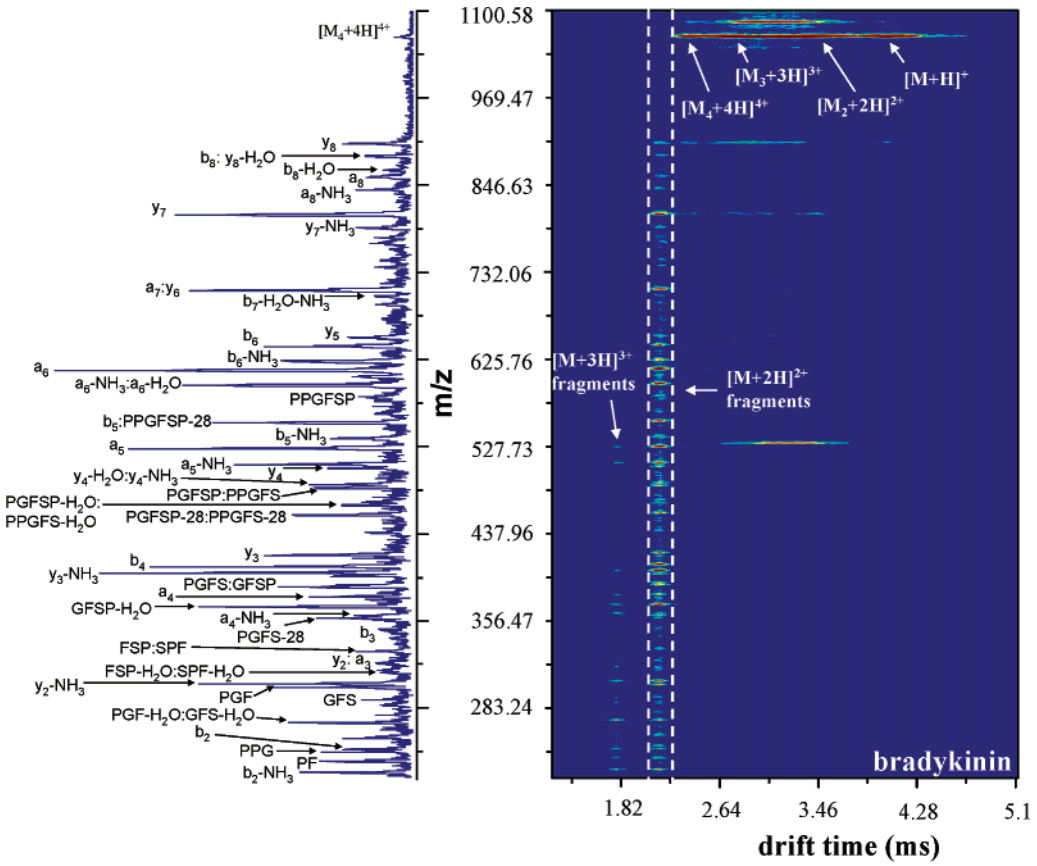

Figure 4. Contour plot of a nested, fragment ion data set for electrosprayed bradykinin ions. Fragmentation is acheived by using high-field collisional activation at the back of the drift tube as illustrated in Figure 2. Singly charged monomer and multimer ions are labeled. Fragments from doubly and triply charged monomer ions are labeled also. On the left is the mass spectrum obtained by summing all drift time bins, within the drift range distinguished by the dashed white lines, at given *m*/*z* values. This range contains the mobility-labeled fragment ions formed at the back of the drift tube from the doubly charged monomer ion (see text). Fragment ion assignments are listed near corresponding peaks.

negligible. The entrance and exit orifices associated with the drift tube are 0.10 and 0.25 cm in diameter, respectively.

The stacked lens assembly allows voltages to be applied from the outside of the drift tube, and we have explored a number of different lens−voltage configurations; however, we focus here on a configuration that is especially well suited for generating fragment ions after precursor ions have been separated by differences in their mobilities. In this configuration, the low-field portion of the drift tube is defined by 12 equally spaced ring electrodes that are connected by a series of 5.00-MΩ high-vacuum resistors (±1%, from KDI Electronics, Whippany, NJ). The last ring in the low-field region (located 1.91 cm from the exit of the drift tube) is covered with a Ni mesh grid (90% transmittance from Buckbee-Mears, St. Paul, MN); this ensures the uniformity of the field along the axis in this region. All of the experiments shown below were carried out using a field of ~5 V·cm^{-1} to separate precursor ions. The shorter, high-field portion of the drift tube (from the grid to the exit orifice) is operated with a nonuniform field that is created by a combination of voltages applied to a stainless steel conical lens and the BeCu exit plate. This is described in more detail below.

RESULTS AND DISCUSSION

Variations in Equipotential Lines in the Second Drift-Field Region. Figure 2 shows SIMION plots of the equipotential lines obtained upon applying two different voltage configurations to the second field region and conical lens assembly.[41] The low-field configuration utilizes a drop of 20 V between the grid/conical lenses and the BeCu exit plate (this region will hereafter be denoted grid/conical lens assembly). This creates what we refer to as a "punch-through" field, which balloons out from the exit hole into the drift tube. This nonuniform field is significant in that it acts as a high-pressure focusing region; however, as shown below, the field is not of sufficient magnitude to induce significant dissociation. When the voltage drop between the conical lens/grid assembly and the BeCu exit hole is increased to 225 V, a much stronger and highly focusing field is generated. As discussed below, this field can be tuned over a wide range of voltages to generate different fragmentation patterns.

Split-Field Drift(Flight) Time Distributions for Electrosprayed Bradykinin. Figure 3 shows a nested drift(flight) time distribution obtained using two split-field voltage configurations for a mixture of bradykinin ions produced by ESI. When 20 V is applied across the grid/conical lens assembly, large peaks in the drift(flight) time distribution at $t_D = 2.31$ and 1.90 ms that can be assigned to the $[M + 2H]^{2+}$ and $[M + 3H]^{3+}$ charge states of intact bradykinin, respectively, are observed. We also see evidence for the $[M + H]^+$ ion as well as several $[M_n + nH]^{n+}$ (multiply charged multimer ions, where $n = 2$ and 3) as reported previ-

(41) Dahl, D. A. *SIMION (Version 7.0)*: Idaho National Engineering Laboratory: Idaho Falls, ID.

ously.[42] Overall, these results are typical of results for this system.[42,43]

A second example of a split-field drift tube data set obtained upon increasing the second field voltage to 205 V is shown in Figure 4. This data set shows evidence for many different ions at drift times of 2.15 and 1.78 ms. These new peaks correspond to fragments of the $[M + 2H]^{2+}$ and $[M + 3H]^{3+}$ precursors. In this case, the remaining precursor ions and fragments arrive at slightly shorter drift times (0.16 and 0.12 ms, respectively) than were observed in Figure 3 because ions are accelerated through a larger potential drop at the back of the drift tube. The observation that precursor and fragments arrive at the same drift times indicates that fragmentation must take place near the exit of the drift tube (the region of highest field). A comparison of the flight times (converted to mass-to-charge ratios) for these ions to fragment ions that are expected for bradykinin allows us to assign peaks to specific ions. We note that in addition to the a-, b-, and y-type fragments that we typically observe upon collisional activation in the skimmer cone region or octopole collision cell,[31,44,45] we observe an increase in the relative abundances of a-type fragment ions as well as a series of new ions (internal fragments).

Figure 5 shows several additional fragmentation mass spectra that are obtained from activating ions upon applying potentials of 50, 180, 250, and 270 V to the grid/conical lens assembly. These data are obtained by integrating a narrow region of each data set that corresponds to the arrival time of the $[M + 2H]^{2+}$ precursor; data for other ions such as the $[M + 3H]^{3+}$ (and several other ion systems that we have tested) appear similar. At low potentials, the mass spectrum is dominated by the $[M + 2H]^{2+}$ precursor. As the potential drop in the second drift-field region is increased to ~120 V (not shown), we observe a distribution of small peaks which correspond to the b-, y-, and a-type fragment ions. These features correspond primarily to cleavage of the peptide backbone and are routinely observed under low-energy activation conditions.[1,8,11,28,29] As the voltage is increased, these peaks dominate the spectrum. The example shown using 180 V shows large peaks associated with the y_8, y_7, and b_6 ions; ~50% of the parent ions appear to have dissociated.

As the voltage is increased beyond 180 V, peaks associated with the series of large a-, b-, and y-type ions decrease in relative intensity and a new series of small peaks are observed. These peaks are readily assigned to several new fragments (e.g., GFSPF, GFSPF-28, and GFSP, as well as smaller a_n- and a_n-NH_3 ions) that are often observed for bradykinin under higher energy activation conditions. At 270 V, the distribution begins to shift and smaller fragments (having lower m/z ratios) are observed. Under our highest voltage conditions, it appears that it is possible to eliminate all fragments containing more than ~5 residues.

Table 1 contains a summary of all the different ions observed and their relative abundances when using four different potentials (50, 180, 250, and 270 V) applied to the grid/conical lens assembly. The data obtained at 50 V are dominated by the $[M + 2H]^{2+}$ parent. At 180 V, the distribution of fragments appears similar to data that we record using on octopole collision cell. Here the largest peak corresponds to the $[M + 2H]^{2+}$ parent—the y_8, y_7, and b_6 fragments are significant having relative abundances of 19, 14, and 18% of the parent ion intensity. By 250 V, the parent ion peak has decreased in intensity and many small fragments are apparent. At still higher voltages (270 V), many of the largest fragments disappear and the distribution is dominated by smaller fragments. Presumably at high voltages the precursor ion forms primary fragments and these undergo additional fragmentation. These data show that very efficient dissociation can be generated. Overall it is possible to control the degree of fragmentation to a remarkable degree.

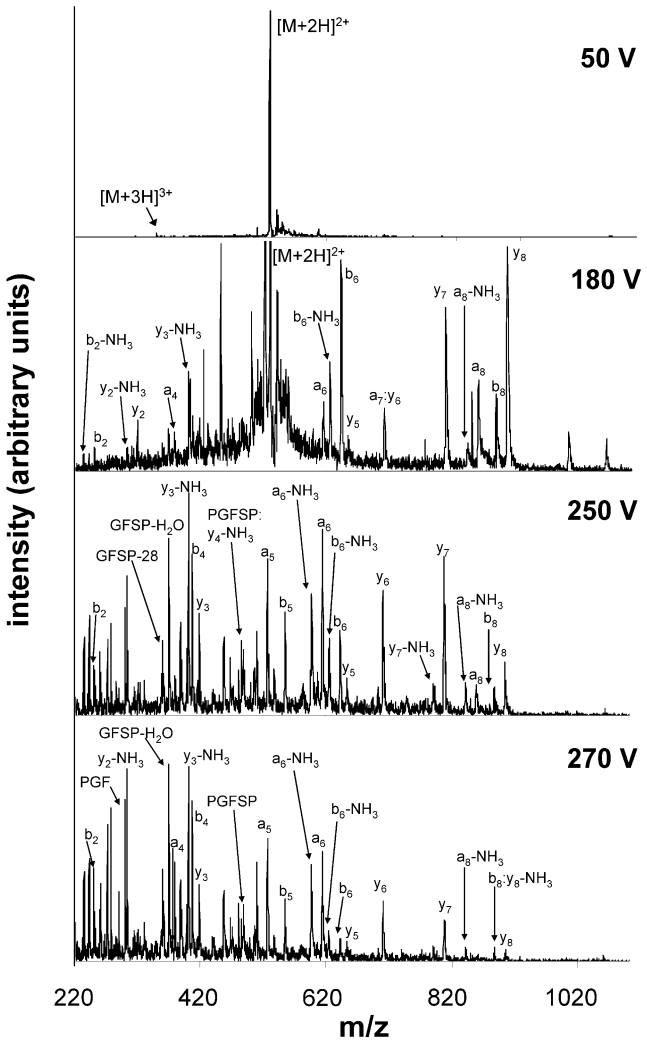

Figure 5. Mass spectra obtained from mobility slices (see Figure 4) for the doubly charged monomer ion of bradykinin. The data were obtained from two-dimensional data sets of electrosprayed bradykinin ions using grid/conical lens potentials of 50, 180, 250, and 270 V from top to bottom. Peaks corresponding to the doubly charged monomer as well as fragment ions are labeled. For a detailed list of fragment ions produced under high- and low-field CID conditions see Table 1.

Example Split-Field Separation and Fragmentation of Multiple Charge States of Electrosprayed Myoglobin. It is interesting to extend this approach to a larger protein ion system. Here, we have injected myoglobin ions into the drift tube using an injection energy of 136 V; under these conditions, the heme is

(42) Counterman, A. E.; Valentine, S. J.; Srebalus, C. A.; Henderson, S. C.; Hoaglund, C. S.; Clemmer, D. E. *J. Am. Soc. Mass Spectrom.* **1998**, *9*, 743−759.

(43) Wyttenbach, T.; Kemper, P. R.; Bowers, M. T. *Int. J. Mass Spectrom.* **2001**, *1*−*3*, 212.

(44) Hoaglund-Hyzer, C. S.; Li, J.; Clemmer, D. E. *Anal. Chem.* **2000**, *72*, 2737.

(45) Hoaglund-Hyzer, C. S.; Lee, Y. J.; Counterman, A. E.; Clemmer, D. E. *Anal. Chem.* **2002**, *74*, 992−1006.

Table 1. Relative Abundance of Different Fragments Produced by CID at the Back of the Drift Tube

m/*z*	ion[a,b]	50 V[c]	180 V	250 V	270 V	*m*/*z*	ion[a,b]	50 V[c]	180 V	250 V	270 V
1061.2	$[M+2H^+]^{2+}$	100	100			506.59	y_4			21	18
905.05	y_8		19	24	5.7	489.56	y_4-NH_3		4.1	30	29
888.02	y_8-NH_3				7.0	486.55	PGFSP, PPGFS		4.4	34	22
887.04	b_8		6.5	13	4.5	468.54	$PGFSP-H_2O$, $PPGFS-H_2O$			26	22
859.03	a_8		7.6	14		458.54	PGFSP−28, PPGFS−28			35	36
841.99	a_8-NH_3		2.3	15	7.0	419.51	y_3		4.4	46	39
807.93	y_7		14	71	85	408.48	b_4		4.6	73	82
790.9	y_7-NH_3		1.4	12	7.6	402.48	y_3-NH_3		8.3	100	99
789.92	y_7-H_2O			14		399.47	PPGF			30	29
739.86	b_7				5.7	391.45	b_4-NH_3			25	26
722.83	b_7-NH_3		1.3			389.43	PGFS, GFSP			42	41
712.83	$PPGFSPF-H_2O$			31		380.47	a_4		3.3	18	50
711.85	a_7		5.2		20	371.42	$PGFS-H_2O$, $GFSP-H_2O$		3.6	80	100
710.82	y_6		5.0	56	31	363.44	a_4-NH_3		2.0	17	31
702.84	PPGFSPF-28		1.4	13	6.3	361.42	PGFS−28, GFSP−28		2.3	34	47
653.76	y_5		3.0	17	10	322.39	y_2		4.2	15	16
642.74	b_6		18	39	12	314.37	$SPF-H_2O$, $FSP-H_2O$			8.2	12
625.71	b_6-NH_3		9.2	35	11	305.36	y_2-NH_3		1.9	63	98
624.72	b_6-H_2O		6.9		15	302.36	PGF			48	82
614.73	a_6		5.8	84	55	292.32	GFS			12	35
597.7	a_6-NH_3			55	49	274.35, 274.3	PGF-28, $GFS-H_2O$			34	69
555.66	b_5		8.5	47	32	254.31	b_2		2.0	20	25
538.63	b_5-NH_3			21	12	252.3	PPG			23	45
536.61	GFSPF				5.1	245.3	PF			45	52
527.65	a_5			70	62	237.28	b_2-NH_3		1.4	35	45
510.62	a_5-NH_3			37	50	235.26	FS				12
508.6	GFSPF-28			16	10						

[a] *m*/*z* ratios were obtained from the MS-Product program on the Protein Prospector web site (http://prospector.ucsf.edu). Average peptide masses were used. [b] Multiple assignments are listed for isobaric and unresolvable peptide ions. [c] Potentials listed are those applied to the last drift tube ring and the conical lens.

lost for most ions and the apomyoglobin polypeptide chain favors the formation of extended structures (as described previously).[46−49] These extended shapes show up as relatively sharp peaks and can be separated in the low-field portion of the drift tube based on differences in charge state.

Figure 6 shows a nested drift(flight) time distribution for several charge states of electrosprayed myglobin ions that have been exposed to high fields (a potential drop of 250 V in the second drift-field region). Under these conditions, it is possible to separate and induce fragmentation in several of the charge states, including nearly all of the charge states that are shown. We note that the $[M + 11H]^{11+}$ and $[M + 10H]^{10+}$ ions do not undergo substantial fragmentation. Figure 7 shows mass spectra obtained for drift time slices comprising the $[M + 15H]^{15+}$ charge state. The data are obtained from three nested data sets that were recorded with conical lens/grid assembly potentials of 40, 200, and 230 V. The parent ion ($[M + 15H]^{15+}$) dominates the spectrum when an applied voltage of 40 V is used. A substantial increase in voltage is required for the onset of fragmentation of this charge state. At 200 V, several fragment peaks are observed. Several features from the two-dimensional data sets have been tentatively assigned to some myoglobin fragments based on the measured *m*/*z* ratios and some comparisons to data published by others.[50] When 230 V is applied, many new fragment ions are produced, so many that there is an overall rise in the baseline of the mass spectral slice. Figure 6 shows that this rise does not result from random noise events but rather from the increased production of numerous fragment ions coincident in drift time with the precursor +15 charge state. As observed for bradykinin, increasing the field at the exit region of the drift tube increases the amount of fragmentation as well as the diversity of fragment ions observed. Protein ion CID data sets are also highly reproducible.

High Fields without Buffer Gas Breakdown. One final comment regards an observation about the present split-field configuration that is somewhat surprising. We find that it is possible to apply very high fields in the second drift-field region −substantially higher than the maximum field of ∼18.5 $V \cdot cm^{-1}$ that can be applied in the first field region, which is limited by breakdown of the buffer gas. At least two explanations may account for the ability to reach higher fields near the exit hole. The pressure near the exit hole (which is near the differentially pumped orifice skimmer region) should be slightly less than that in the first field region of the drift tube; lower pressures may allow the field to increase near the hole without initiating a discharge causing the gas to breakdown. In this case, the pressure is expected to decrease slightly near the exit hole (where the gas is being pumped away). The field increases as one approaches the exit region; however, it is possible that the decrease in pressure raises the breakdown potential enough to apply relatively high fields (∼1750 $V \cdot cm^{-1}$ near the exit). Additionally, we note that although the ballooning shape of the field should aid in

(46) Clemmer, D. E.; Hudgins, R. R.; Jarrold, M. F. *J. Am. Chem. Soc.* **1995**, *117*, 10141.
(47) Shelimov, K. B.; Jarrold, M. F. *J. Am. Chem. Soc.* **1996**, *118*, 10313.
(48) Shelimov, K. B.; Clemmer, D. E.; Hudgins, R. R.; Jarrold, M. F. *J. Am. Chem. Soc.* **1997**, *119*, 2240.
(49) Woenkhaus, J.; Mao, Y.; Jarrold, M. F. *J. Phys. Chem. B* **1997**, *101*, 847.
(50) Newton, K. A.; Chrisman, P. A.; Reid, G. E.; Wells, J. M.; McLuckey, S. A. *Int. J. Mass Spectrom.* **2001**, *212*, 359.

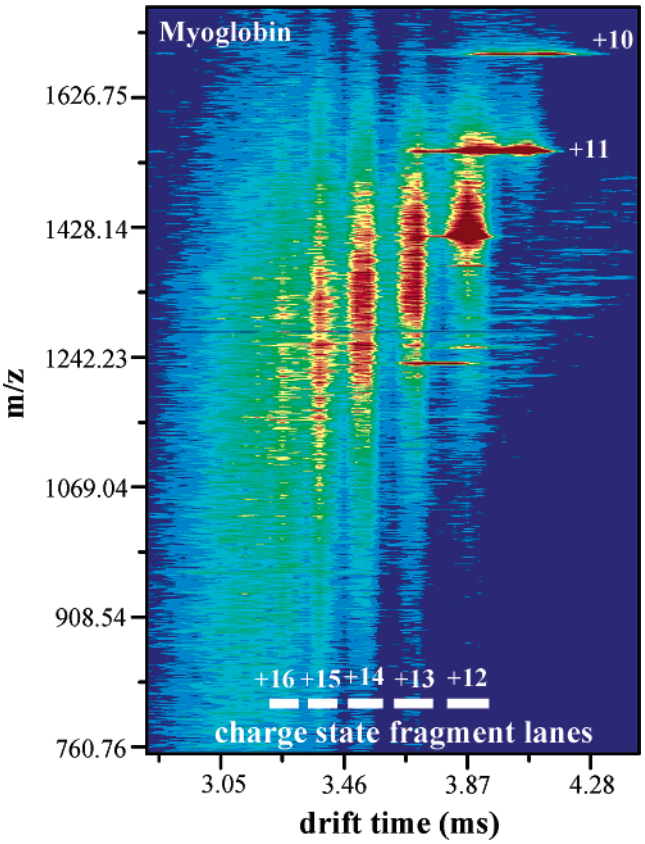

Figure 6. Contour plot of a nested, fragment ion data set for myoglobin ions. Features corresponding to the M^{10+} and M^{11+} ions formed by proton-transfer reactions (see text) are labeled. Also shown are charge-state "fragment lanes" with multiple mobility-labeled fragment ions formed using high-field collisional activation (see Figure 2) of the myoglobin charge states listed. See text for more details.

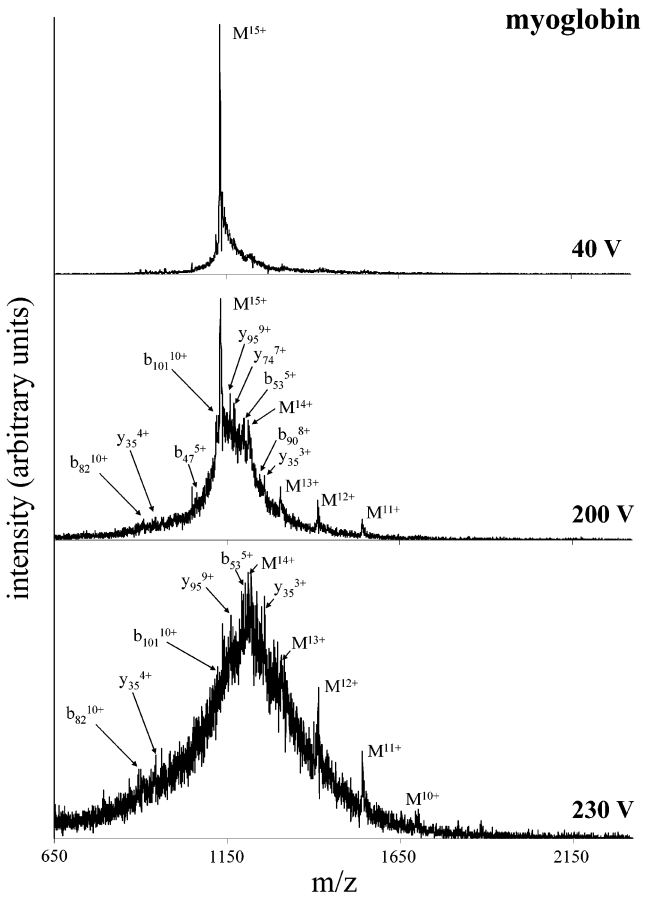

Figure 7. Mass spectra obtained from mobility slices of the M^{15+} charge state of electrosprayed myoglobin ions. The data were obtained from two-dimensional data sets recorded using grid/conical lens potentials of 40, 200, and 230 V for the top, middle, and bottom traces, respectively. Several multiply charged monomer peaks are labeled, and some tentative fragment assignments are also given.

focusing positively charged ions out of the drift tube, any electrons that are formed at high fields would be defocused. In this case, if electrons were formed (as would be required to initiate a discharge), they would likely not travel down the axis of the drift tube. Instead, electron trajectories would track the defocusing fields and are likely to collide with the inside surface of the conical lens. In this case, it is possible that spurious electrons are detached from the buffer gas; however, conditions do not appear to allow a sustained discharge to occur. We note that the latter explanation is speculative; we also see no evidence for additional current through the circuit, which would suggest a local sustained discharge.

SUMMARY AND CONCLUSIONS

A new split-field drift tube design has been presented. The approach provides a means of separating mixtures of precursor ions based on differences in their mobilities and subsequently inducing fragmentation in the second field region. Dissociation inside the drift tube is highly efficient, and it is possible to tune fields to generate different fragmentation patterns without significant loss in ion signal. The approach also appears to be versatile, and an example showing the dissociation of electrosprayed bradykinin as well as a distribution of charge states for electrosprayed myoglobin ions has been presented. We note that this experimental configuration is very simple to build and operate; such a simple configuration should be useful to a wide range of chemical problems where parent ion mobility, mass and fragmentation information is desired. Further work in our laboratory is underway in order to further refine fields with the aim of providing more detailed control of the collision-induced dissociation process.

ACKNOWLEDGMENT

This work is supported by grants from the National Science Foundation (CHE-0078737) and National Institutes of Health (1R01GM-59145-03). We are also grateful for support from the Indiana Genomics Initiative (INGEN), which has funded some instrument development in our group that is related to this work.

Received for review March 18, 2003. Accepted August 27, 2003.

AC030111R